# Multidisciplinary Analysis of Aero-Propulsive Coupling for the OWN Concept

Jai Ahuja*, S.Ashwin Renganathan †, Steven Berguin ‡
and Dimitri N. Mavris§
*Georgia Institute of Technology, Atlanta, GA, 30332, USA*

**The Over Wing Nacelle (OWN) concept enables the installation of turbofans with high bypass ratios for improved efficiency in commercial transport vehicles, in addition to offering other advantages in the form of (i) mitigation of jet noise, (ii) foreign object damage avoidance and (iii) jet-powered lift. While these benefits can be offset by the large transonic drag rise, aerodynamic shape optimization of the wing and nacelle outer mold lines can help realize the full aerodynamic potential of the OWN concept. However, if coupling between the airframe aerodynamics and the propulsion system is strong, multidisciplinary optimization may need to be conducted. In this paper, the aerodynamics-propulsion coupling in the OWN concept is studied. A high fidelity Reynolds Averaged Navier Stokes (RANS) model along with a low fidelity engine thermodynamic cycle analysis model are used to represent the aerodynamic and propulsion systems respectively. The necessary coupling variables are identified and the coupled system is solved for disciplinary feasibility using the Fixed Point Iteration technique. The Common Research Model (CRM) wing and nacelle are used as the baseline geometry to carry out the study. The study reveals that for the OWN concept, aerodynamics-propulsion coupling is not significant enough to warrant multi-disciplinary shape optimization. While airframe aerodynamics has a strong effect on the propulsion system, the reverse interaction is weaker.**

## Nomenclature

| | |
|---|---|
| $A$ | Area |
| $C_D$ | Drag coefficient |
| $C_L$ | Lift coefficient |
| $F_N$ | Net thrust |
| $\dot{m}$ | Mass flow rate |
| $M$ | Mach number |
| $P$ | Pressure |
| $T$ | Temperature |
| $\mathbf{Y}_{AP}$ | Vector of coupling variables required by propulsion from aerodynamics |
| $\mathbf{Y}_{PA}$ | Vector of coupling variables required by aerodynamics from propulsion |
| $\eta_{PR}$ | Pressure recovery - ratio of the fan face stagnation pressure to the ambient stagnation pressure |

*Subscripts*

| | |
|---|---|
| $A$ | Quantities obtained from aerodynamics |
| $P$ | Quantities obtained from propulsion |
| $t$ | Stagnation properties |
| 0 | Station: Ambient |
| 1 | Station: Inlet highlight plane |
| 2 | Station: Fan face |
| 8 | Station: Core nozzle inlet |
| 18 | Station: Bypass nozzle inlet |

*PhD Candidate, Aerospace Systems Design Laboratory, and AIAA Student Member.
†Postdoctoral Researcher, Aerospace Systems Design Laboratory, and AIAA Student Member.
‡Research Engineer II, Aerospace Systems Design Laboratory, and AIAA Student Member.
§Boeing Professor of Advanced Aerospace Systems Analysis, School of Aerospace Engineering, AIAA Fellow

# I. Introduction

The need for more efficient engines to meet the next generation NASA $N+2$ and $N+3$ emission and fuel burn targets [1] for commercial transport vehicles can be addressed with Ultra High Bypass Ratio turbofan engines [2, 3]. Bypass ratio for under-wing mounted engines is constrained by ground clearance and landing gear weight. An over-wing installation of the engine eliminates these constraints and comes with the added benefit of fan and/or jet noise shielding by the wing. However, wing-nacelle interference is exacerbated, resulting in an increased transonic drag penalty. On the other hand, past studies [4, 5] have reported that upon identifying a suitable installation location and optimizing the wing and nacelle outer mold lines, superior aerodynamic performance can be obtained compared to the corresponding under-wing baseline. Therefore, aerodynamic shape optimization (ASO) of the engine installed wing is critical in order to realize the full potential of the Over-Wing Nacelle (OWN) aerodynamic performance.

Key aspects of the OWN concept are (i) jet scrubbing on the wing upper surface leading to aerodynamic interference in the form of powered lift [6, 7] for configurations where the engine is placed at the wing leading edge and (ii) engine inflow interference that can lead to losses in inlet pressure recovery for a trailing edge configuration. To account for such phenomena in the optimization problem, the engine has to be modeled under *power-on* conditions. This implies imposing thermodynamic boundary conditions on the engine fan, and bypass & core nozzle inlet faces in the CFD model. ASO with fixed powered boundary conditions might not account for the impact of the propulsion system on the airframe and vice versa. For instance, an optimized wing shape leads to improved airframe drag that lowers the required engine thrust. Modifying the engine thrust however may affect the flow-field over the wing and nacelle, modifying the airframe drag in return. A previous study [8] found statistically significant coupling between the airframe aerodynamics and the propulsion system, but the strength of the coupling, measured in terms of differences in the aerodynamic coefficients calculated with and without coupling, has not been quantified before. The goal of this paper is to address this gap, and in doing so hopes to answer the question: is Multidisciplinary Design Analysis and Optimization (MDAO) necessary for an OWN trailing edge configuration, or is a decoupled approach, where ASO is conducted with the engine at a fixed power setting, sufficient?

This paper combines Reynolds Averaged Navier Stokes (RANS) analysis and a low-fidelity engine cycle model to perform a multidisciplinary analysis (MDA) of the OWN configuration at different angles of attack. A methodology to properly account for interdisciplinary coupling and solve the resulting MDA problem is presented. The Common Research Model (CRM) [9, 10] wing and nacelle are used as the baseline geometry for this analysis. The CRM nacelle is modified by extracting a longitudinal section that is revolved 360 degrees to give an axisymmetric fan cowl, and a 2D flowpath for the engine core is revolved that snugly fits into the fan cowl. A simplified model of the powered engine is developed by specifying appropriate boundary conditions at the fan face and the bypass & core nozzle inlets. The engine is sized using the NASA Environmental Design Space (EDS) [11] that combines aircraft mission analysis, engine thermodynamic cycle analysis and performance analysis tools. The sized engine is run at various throttle settings at cruise and and the boundary conditions necessary are extracted from the cycle analysis. Surrogate models for the boundary conditions are developed for easier integration within the MDA framework.

The following section presents an overview of the MDA methodology and comments on the geometry, analysis models and framework used to solve the problem. Results presented look into trends of key aerodynamic and propulsion outputs as a function of angle of attack and comment on the differences observed as a result of capturing the coupling. The paper concludes with a summary of results and an outlook on future work.

# II. Methodology

## A. MDA Problem Formulation

Capturing interdisciplinary feedback in the design process requires an understanding of the disciplinary analysis workflow for propulsion and aerodynamics; specifically the variables that are shared between the various disciplines (also known as coupling variables) need to be identified. Engine cycle analysis typically works with stagnation pressures and temperatures. At ambient conditions, known static temperature and pressure values ($T_0$, $P_0$) are converted to stagnation values through isentropic relations. Assuming no heat or work addition to the flow from ambient conditions, the stagnation temperature at the fan face ($T_{t_2}$) is the same as that in the freestream ($T_{t_0}$) for a calorically perfect gas. The stagnation pressure at the fan

face is obtained from $\eta_{PR} P_{t_0}$. $\eta_{PR}$ is the pressure recovery term capturing the stagnation pressure losses in the flow leading up to the fan face. Strictly speaking, $\eta_{PR}$ only characterizes the inlet pressure losses i.e. $\eta_{PR} = P_{t_1}/P_{t_0}$ where $P_{t_1}$ is the stagnation pressure at the inlet highlight plane. For under-wing mounted engines on subsonic transports, pressure losses in the freestream flow are negligible and $P_{t_0} = P_{t_1}$ can be assumed. For OWN trailing edge configurations however, a shock on the upper surface of the wing presents an additional source of pressure loss and $P_{t_0} \neq P_{t_1}$. Instead of calculating $P_{t_1}$ separately, it is more convenient to lump all stagnation pressure losses leading up to the fan face in $\eta_{PR}$.

Net thrust produced by the engine at cruise must equal the total airframe drag, and this is achieved by altering the fuel flow rate, controlled by the throttle setting. For a given thrust required and known thermodynamic properties at the fan face, a turbomachinery matching process is employed to ensure that the power produced by the turbine balances the power requirements of the fan and compressors. Engine performance, thermodynamic properties at the stations downstream of the fan face, and the mass flow rate required by the engine are a fallout of this matching process. Essentially, the state of the engine at cruise is governed by two parameters: airframe drag ($C_D$) and pressure recovery. These values can be obtained from CFD analysis of the engine-installed airframe.

Modeling the airframe-engine combination in CFD requires imposing boundary conditions on the engine faces where flow leaves and enters the fluid domain. The fan face is modeled as a pressure outlet in CFD and requires specification of the static pressure and temperature ($P_2$ and $T_2$). That being said, only $P_2$ is an independent boundary condition that can be controlled. $T_2$ is a fallout of the flow solution and the imposed temperature boundary condition will be adjusted by the CFD solver as necessary. Additionally, the bypass and core nozzle inlet planes are modeled as stagnation inlets and require the specification of stagnation conditions $P_{t_{18}}$ and $T_{t_{18}}$ for the bypass inlet, and $P_{t_8}$ and $T_{t_8}$ for the core inlet. These boundary conditions are obtained from the engine cycle analysis.

In MDAO terminology, $C_D$ and $\eta_{PR}$ are the coupling variables required by the engine cycle, calculated by CFD (denoted by $\mathbf{Y}_{AP}$), while $P_2$, $P_{t_{18}}$, $T_{t_{18}}$, $P_{t_8}$, and $T_{t_8}$ are the coupling variables required by CFD, calculated by the engine cycle analysis (denoted by $\mathbf{Y}_{PA}$). For this aero-propulsion coupled system, any changes to $\mathbf{Y}_{AP}$ results in changes to $\mathbf{Y}_{PA}$ and vice versa. This interaction between the airframe and the propulsion system can be represented by a coupled system of equations that needs to be solved iteratively to obtain the multi-disciplinary converged solution. This iterative process ends when the change in the coupling variables between iterations is less than some tolerance.

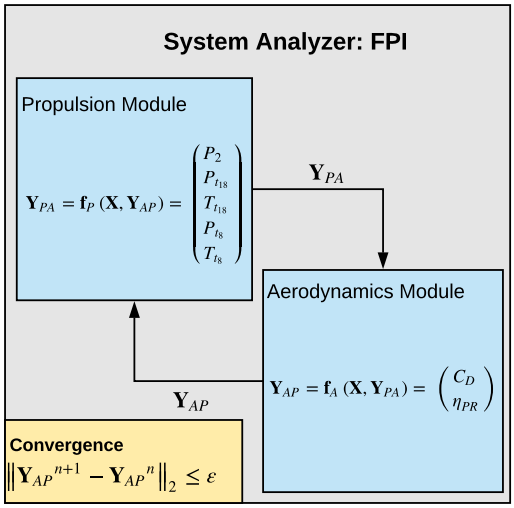


Figure 1: Illustration depicting the coupled aero-propulsion analysis problem. *The process begins with providing a starting guess for the aerodynamics coupling variables to the propulsion module. A set of engine boundary conditions are calculated for this guess, which are then used by the aerodynamics module to calculate the updated values of the airframe drag and pressure recovery. These are passed back to the propulsion module and the process repeats till the convergence condition is met. This procedure is the commonly used Fixed Point Iteration (FPI) algorithm.*

*Comments on Matching Mass Flow Rate at the Fan Face*

For OWN trailing edge configurations, airflow over the wing is affected by the mass flow rate required by the engine. It is thus important to match the flow rate entering the fan face, as calculated in CFD ($\dot{m}_{2_A}$), with the requirements presented by the engine cycle analysis ($\dot{m}_{2_P}$). Fidelity differences between the engine cycle analysis and CFD however make an exact matching difficult. CFD computation of flow rate at the fan face is sensitive to the mesh resolution, flow angularity, and numerical error. Additionally, there are variations in the velocity and thermodynamic properties along the fan face, exacerbated if a RANS simulation is performed due to the presence of boundary layers on the inlet walls. Engine cycle analysis codes assume uniform flow along the axial direction and cannot capture these higher order effects.

$\dot{m}_{2_A}$ in CFD is affected by $P_2$, which is obtained from the cycle analysis code. $P_2$ is a coupling variable explicitly controlled by the MDA solver and thus $\dot{m}_{2_A}$ is implicitly controlled. Mass flow at the fan face can be calculated using Eq. 1.

$$\dot{m}_2 = \rho_2 A_2 V_2 = \eta_{PR} P_{t_0} A_2 M_2 \sqrt{\frac{\gamma}{RT_{t_0}}} \left(1 + \frac{\gamma - 1}{2} {M_2}^2\right)^{-\frac{(\gamma+1)}{2(\gamma-1)}} \tag{1}$$

Pressure recovery measured in CFD is a function of the cycle analysis $P_2$ and CFD calculated averaged Mach number, $M_2$, as seen in Eq. 2.

$$\eta_{PR_A} = \frac{P_2}{P_{t_0}} \left(1 + \frac{\gamma - 1}{2} {M_{2_A}}^2\right)^{\frac{\gamma}{\gamma-1}} \tag{2}$$

For a given thrust required, the mass flow rate required is calculated by the engine cycle code. With the known flow rate and assumed value for pressure recovery, the fan face Mach number in the cycle code can be obtained by solving Eq. 1. Given this value, the cycle analysis calculates the fan face static pressure from Eq. 3.

$$P_2 = \eta_{PR_P} P_{t_0} \left(1 + \frac{\gamma - 1}{2} {M_{2_P}}^2\right)^{-\frac{\gamma}{\gamma-1}} \tag{3}$$

Thus, when the MDA solver reaches a converged solution, i.e. when $\left\| {\mathbf{Y}_{AP}}^{n+1} - {\mathbf{Y}_{AP}}^{n} \right\|_2 \leq \varepsilon$, averaged $M_{2_A} \approx M_{2_P}$. Thus $\dot{m}_{2_A}$ calculated using Eq. 1 will be reasonably close to $\dot{m}_{2_P}$. It is important to note that this comparison depends on the averaged thermodynamic properties at the fan face, with averaging required to account for the uniform flow assumption made by the cycle analysis code. Averaged thermodynamic properties calculated in CFD are still sensitive to the factors mentioned before, as well as the choice of RANS vs. Euler analysis, but reasonable agreement between $\dot{m}_{2_A}$ and $\dot{m}_{2_P}$ is to be expected at the end of the MDA iteration.

## B. Baseline Airframe and Engine

As mentioned earlier, the CRM is used as the baseline wing-body geometry for this study. Accounting for symmetry of the airframe, half the geometry is modeled as shown in Fig. 2.

Figure 2: Wing and powered nacelle geometry

The CRM nacelle has been modified by extracting one longitudinal section and revolving it to obtain an axisymmetric geometry. The nacelle diameter and core engine flow path (see Fig. 3b) are extracted from EDS (see Fig. 3a). The engined is sized for a notional 300 passenger class airplane, like the Boeing 777 for example, and thus has a similar architecture to the GE90-94B engine.

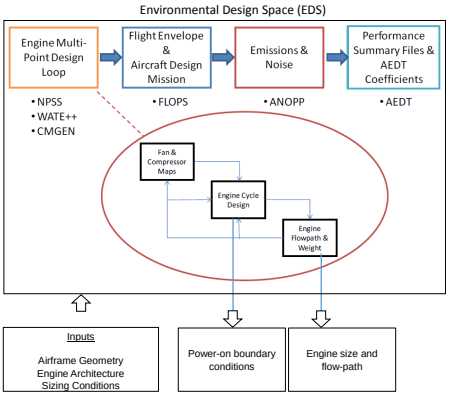


(a) The Environmental Design Space (EDS) framework for propulsion system sizing

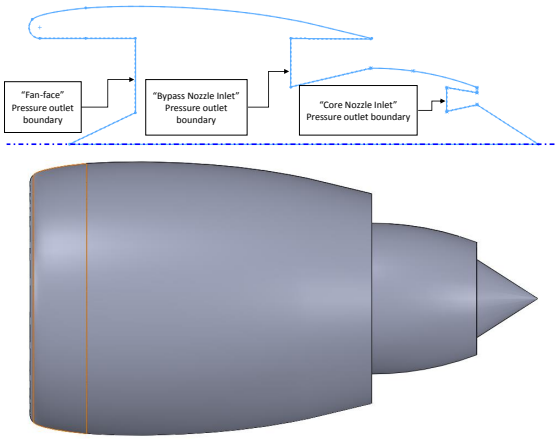


(b) Powered nacelle geometry and boundary conditions

Figure 3: Powered engine sizing tool and geometry

For verification, the isolated powered engine was simulated at cruise conditions, $M = 0.85$ and altitude of 35,000 ft, with zero incidence angle. The purpose was to evaluate the validity of the boundary conditions and the engine geometry extracted from a lower fidelity code for a high fidelity RANS simulation. The computed engine mass flow rates at the three stations where boundary conditions are specified are compared against the EDS values, as shown in Table 1. A small discrepancy between the RANS and EDS predictions is noticed, but this is due to fidelity differences as discussed previously.

Table 1: Comparison of RANS prediction of engine mass flow rates vs EDS

| | EDS | CFD | Error(%) |
|---|---|---|---|
| Fan face massflow rate (lb/s) | 1326.38 | 1312.28 | 1.06 |
| Bypass nozzle massflow rate (lb/s) | 1181.19 | 1154.471 | 2.26 |
| Core nozzle massflow rate (lb/s) | 138.22 | 147.798 | 6.93 |

### C. Engine Surrogate Model

Integration of the engine model with existing aerodynamic tools in the MDA framework is facilitated through the use of surrogate models for the engine boundary conditions. Response surface equations are generated for each boundary condition of the form shown in Eq. 4

$$y = \sum_{j=1}^{m} \beta_j \phi_j(\mathbf{x}) \tag{4}$$

where $y$ represents a single boundary condition, $\mathbf{x}$ is the vector of inputs, which in this case are the aerodynamics coupling variables: net thrust and pressure recovery, and $m$ represents the number of basis functions used. The basis vector used for the surrogates is $\phi = (1, \eta_{PR}, F_{Ns}, \eta_{PR}^2, F_{Ns}^2, F_{Ns}\eta_{PR})$. $\beta_j$ are unknown regression coefficients. The EDS engine model is run in off-design mode for varying values of pressure recovery and net thrust produced and the boundary conditions at each case are recorded. Net thrust is scaled by a reference value to ensure the same scale with pressure recovery. For a given boundary condition, the following linear system is obtained:

$$\begin{pmatrix} y_1 \\ \vdots \\ y_N \end{pmatrix} = \begin{pmatrix} \phi_1(\mathbf{x}_1) & \dots & \phi_6(\mathbf{x}_1) \\ \vdots & \ddots & \vdots \\ \phi_1(\mathbf{x}_N) & \dots & \phi_6(\mathbf{x}_N) \end{pmatrix} \begin{pmatrix} \beta_1 \\ \vdots \\ \beta_6 \end{pmatrix} \quad \Leftrightarrow \quad \mathbf{y} = \mathbf{\Phi}\boldsymbol{\beta} \tag{5}$$

where $N$ represents the number of samples used to generate the surrogate model. The unknown coefficients are found as follows:

$$\boldsymbol{\beta} = (\mathbf{\Phi}^T\mathbf{\Phi})^{-1}\mathbf{\Phi}^T\mathbf{y} \tag{6}$$

Note that in practice, matrix inversion is typically avoided and the linear system in Eq. 5 is solved more efficiently using other techniques such as QR factorization for example. Surrogate models generated for the boundary conditions can be seen in Fig. 4. Red dots in the figure are the points used to fit the surrogates. Good fits are observed for each boundary condition, and thus there is minimal loss in accuracy using these surrogates in the MDA loop instead of EDS.

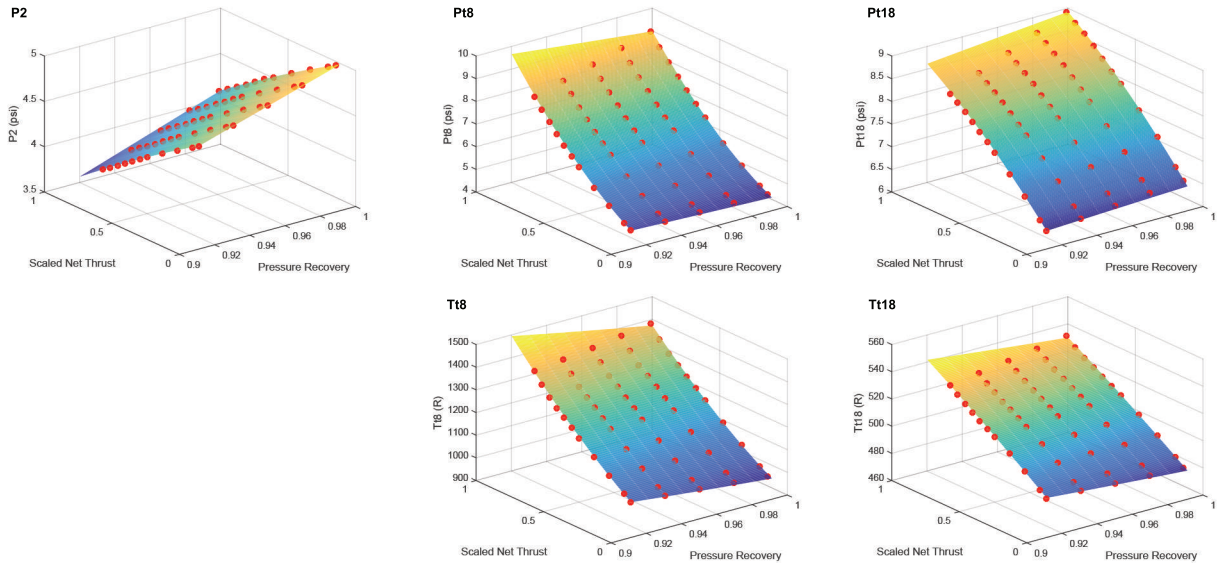


Figure 4: Illustration depicting the responses of the engine boundary conditions to changes in net thrust and pressure recovery. $R^2$ for each response is around 0.99.

## D. CFD Model

All results are generated using the commercial software STAR-CCM+ under fully turbulent, steady-state, Reynolds-Averaged Navier-Stokes (RANS) assumptions. The solver uses a finite volume approach with implicit time integration scheme and 2nd order upwind spatial discretization. The flux at the boundary is reconstructed using Roe flux difference splitting with the Venkatakrishnan limiter. The Courant number is set to 25 and, to accelerate convergence, an Algebraic Multi-Grid (AMG) method is used with 30 V-cycles and a Gauss-Seidel relaxation scheme. A hemispherical flow domain with 30 times the CRM wing-span as radius is discretized with $15 \times 10^6$ polyhedral cells and prism layers to capture the boundary layer development (Fig. 5). The mesh density was carefully adjusted to enable quick solver turnaround times while also maintaining sufficient resolution to capture losses due to shocks and boundary layers.

## E. Framework Setup

The MDA framework developed for this problem is written in python and Java. MDA loop convergence is conducted in Python with a custom FPI script. Aerodynamics and propulsion disciplines are represented by two separate classes, with each class responsible for providing the MDA solver with values of the coupling variables. The propulsion class consists of the engine boundary condition surrogate equations, while the

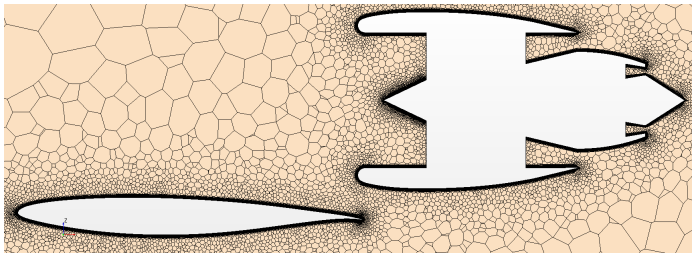

Figure 5: Polyhedral volume mesh (15.4M cells) for the CRM wing-body-nacelle configuration.

aerodynamics class consists of methods used to interact with the CFD software. Interaction with STAR-CCM+ occurs through a Java framework, that leverages as well documented API to automate the CFD process. CFD automation consists of reading in and updating the engine boundary conditions, running the primal flow solver, and outputting key aerodynamic properties. The aerodynamics class in python interacts with this Java framework, acting as a conduit for I/O flow between the CFD software and the MDA solver.

# III. Results

## A. Key Aerodynamic Outputs

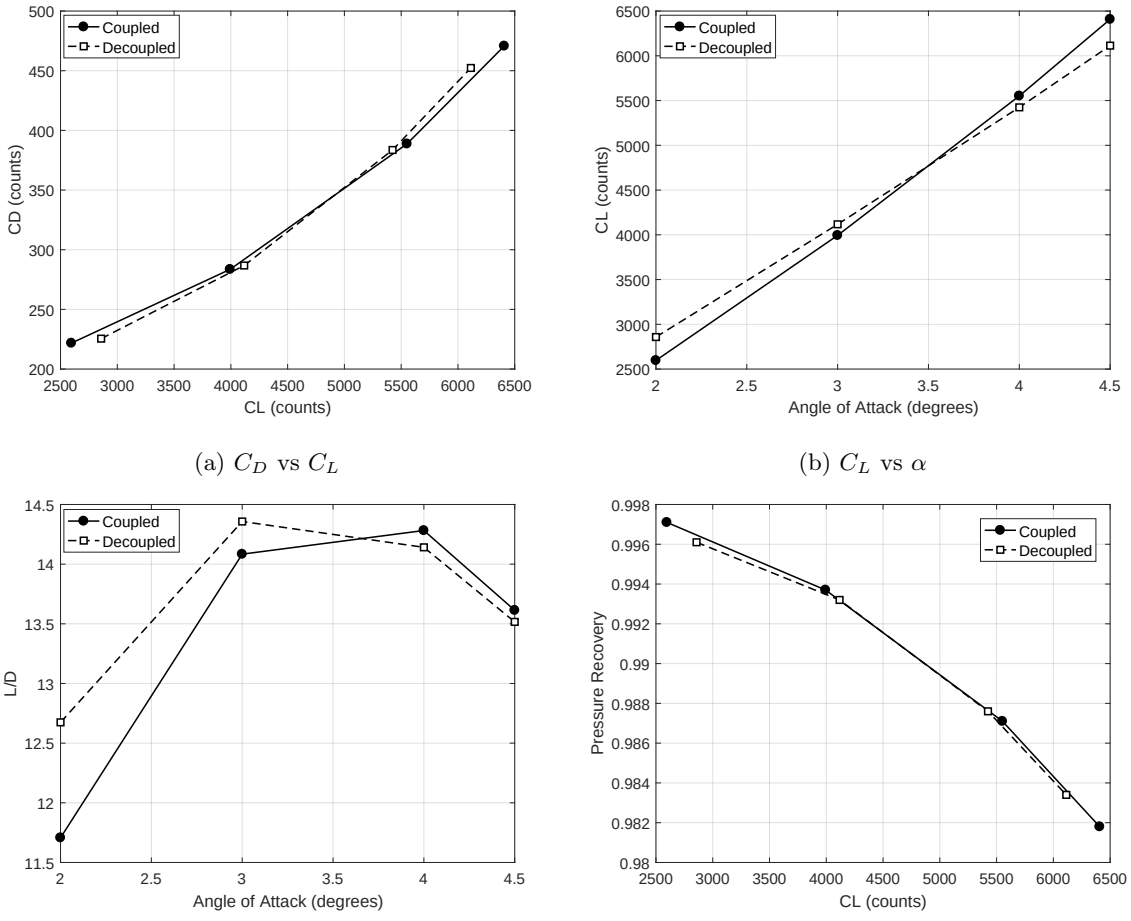


(a) $C_D$ vs $C_L$

(b) $C_L$ vs $\alpha$

(c) $L/D$ vs $\alpha$

(d) $\eta_{PR}$ vs $C_L$

Figure 6: $C_D$, $C_L$, $L/D$, and $\eta_{PR}$ trends as a function of flight condition

Figs. 6a-6d present a comparison between decoupled and coupled trends for $C_D$, $C_L$ and $\eta_{PR}$ for varying angles of attack between 2 and 4.5 degrees. The reason angle of attack is varied to assess coupling strength is two-fold (i) for a given nacelle location, angle of attack is the parameter that is adjusted until the desired flight condition (in terms of $C_L$) is achieved and (ii) depending on the flow incidence angle, the aerodynamic interaction between the propulsion system and airframe is expected to vary and therefore lead to different levels of coupling.

At the outset, it appears that the propulsion system does not have a significant impact on the airframe aerodynamics for this nacelle location. There is a small, but noticeable increase in the lift curve slope (Fig. 6b) as a result of capturing the coupling, which accounts for the difference seen in the $L/D$ trends (Fig. 6c). The difference between coupled and decoupled $C_D$ and $\eta_{PR}$ trends is negligible for the AoA range between 2 and 4.5. Note that the CRM cruise $C_L$ of 0.5 falls in this range. The differences in the trends grow outside this $C_L$ range, but are not significant enough to suggest a strong 2-way aerodynamics-propulsion coupling.

It is important to note that pressure recovery exhibits sensitivity to angle of attack for this configuration. As the angle of attack (and hence lift) is increased, there is greater flow acceleration over the wing. This results in a stronger shock on the upper surface, yielding a larger stagnation pressure drop and thus lower pressure recovery. Therefore, the aerodynamic characteristics of the airframe has a discernible impact on the propulsion system performance through a penalty in $\eta_{PR}$. A loss in pressure recovery by 1-2% deteriorates thrust production and leads to fuel burn penalties for the entire mission in the order of 10,000 - 25,000 lbs (Fig. 7).

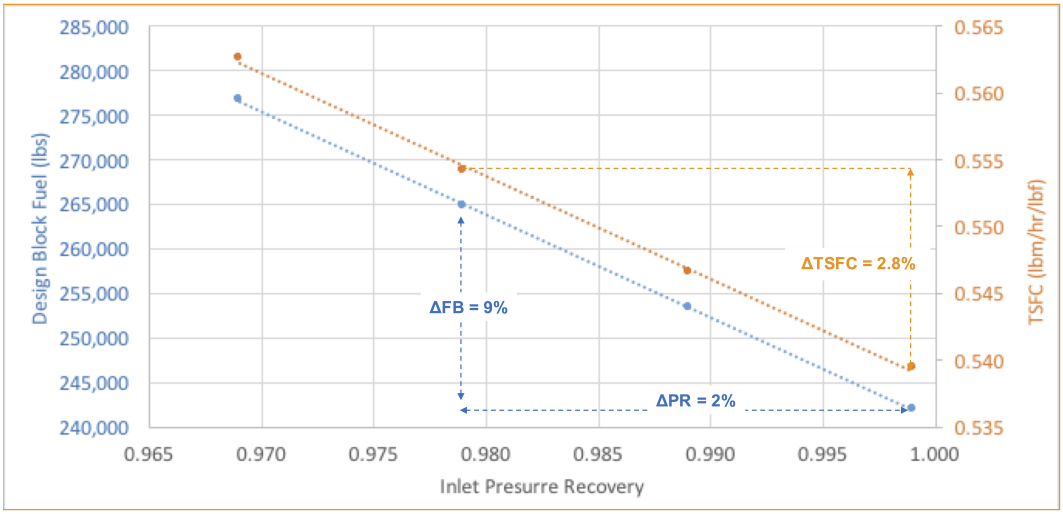


Figure 7: Fuel burn as a function of pressure recovery for a notional 300 passenger class transport and high bypass 94,000 lbs thrust class turbofans (generated using EDS [11])

Moving the engine higher above the wing mitigates pressure recovery loss due to reduced interference with the wing [8]. However, structural limitations constrain the vertical displacement of the engine from the wing since flutter characteristics of the wing for OWN concepts are strongly dependent on the location of the engine and the relative stiffness of the pylon and wing [12]. This tradeoff between propulsion and structures needs to be considered when choosing an optimum nacelle location. Pressure recovery can also be improved by weakening the upper surface shock though aerodynamic shape optimization of the wing.

### B. Comparison of Flow Features

As seen in the preceding subsection, differences in the aerodynamic outputs calculated with and without coupling is small. It is therefore expected that both the decoupled and coupled cases would exhibit similar flow features. Figs. 8a and 8b compare the pressure coefficient contours on the airframe and nacelle from the decoupled and coupled cases for one specific angle of attack at $\alpha = 4.5$, while Figs. 9a and 9b compare the Mach contours at the engine centerline plane at the same angle of attack. No significant differences can be seen in the pressure and Mach contours between the two cases.

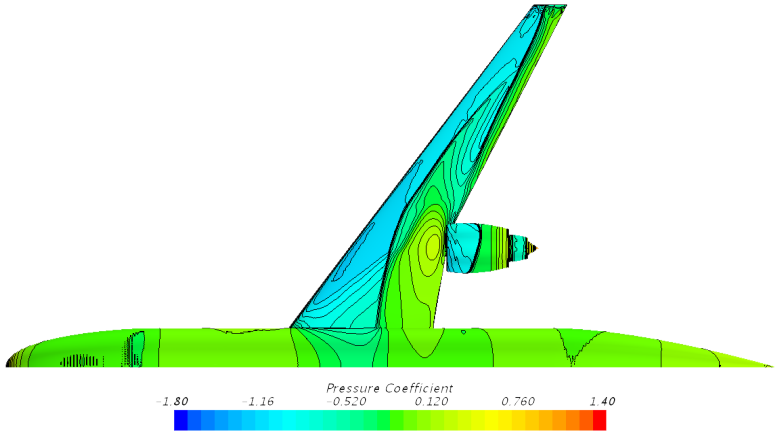


(a) Decoupled

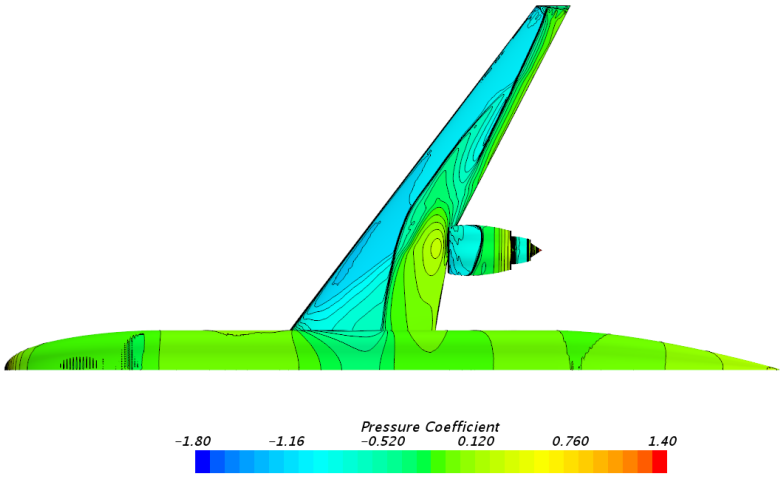


(b) Coupled

Figure 8: Comparison of the $C_p$ contours over the airframe and nacelle at $\alpha = 4.5$

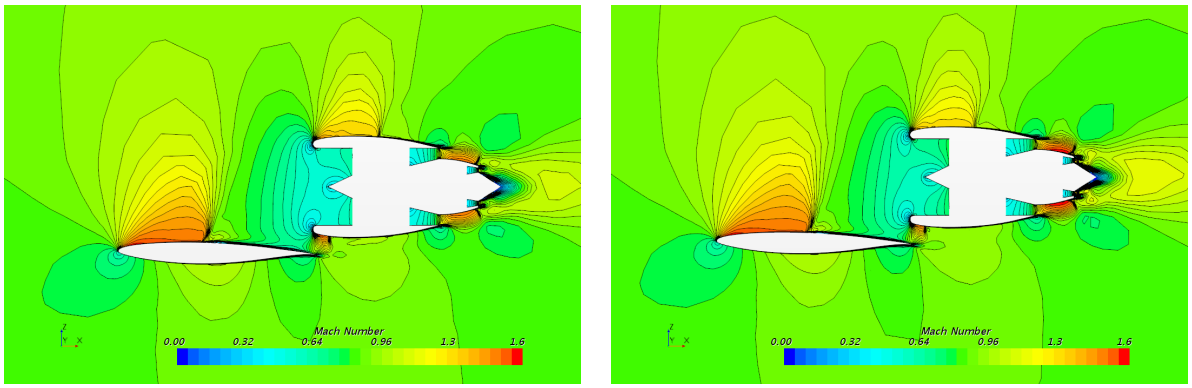


(a) Decoupled

(b) Coupled

Figure 9: Comparison of the Mach number contours at the engine centerline plane at $\alpha = 4.5$

Subtle differences in flow features are highlighted in Fig. 10, which compares the $C_p$ distributions at different stations along the wingspan for the decoupled and coupled cases. Pressure distributions are identical everywhere except in the vicinity of the shock. For stations at 16.4%, 32.8% and 60.9%, the shock from the coupled case is located further downstream relative to the decoupled case. The lower back pressure in the coupled case, generated as a result of changing the engine fan face static pressure in the MDA loop, accounts for this difference.

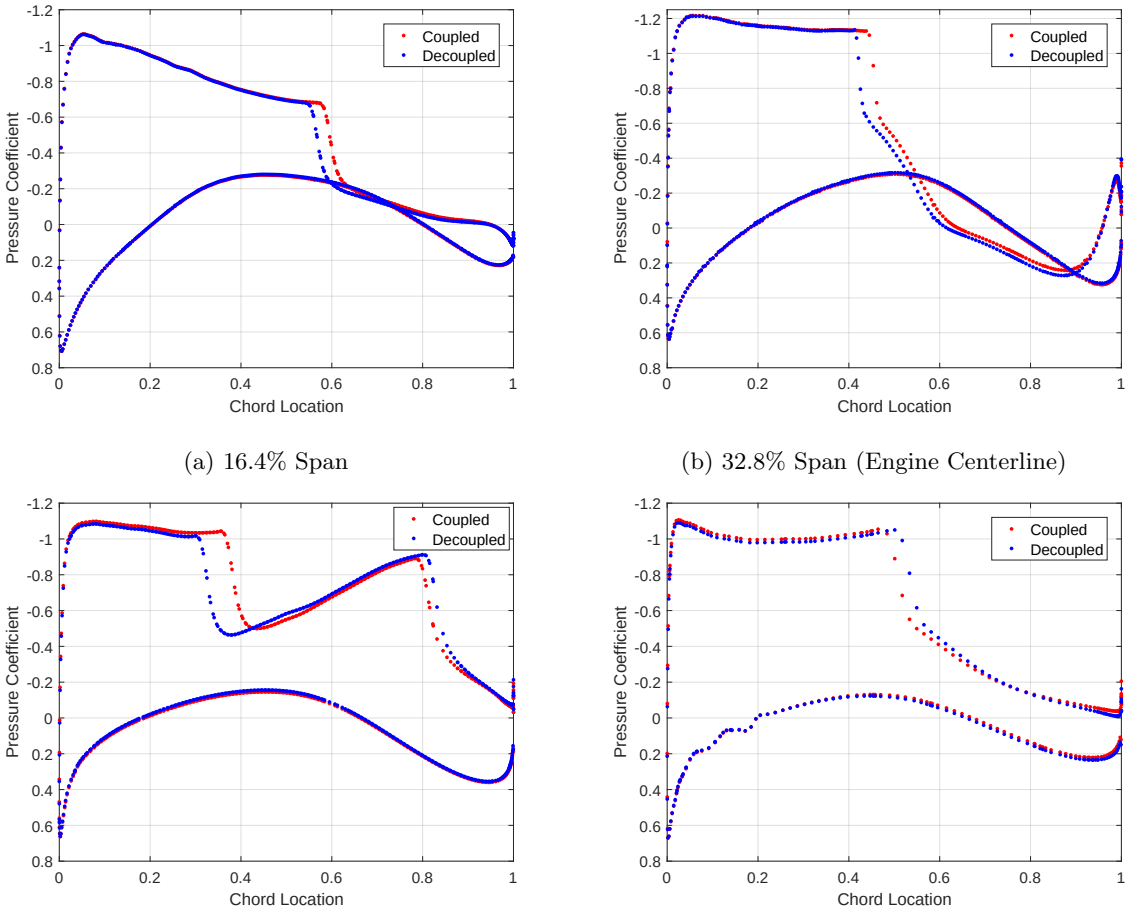


(a) 16.4% Span

(b) 32.8% Span (Engine Centerline)

(c) 60.9% Span

(d) 94.4% Span

Figure 10: Comparison of the decoupled and coupled pressure coefficient distributions at different wing stations for $\alpha = 4.5$

The location of the shock is an important characteristic that defines the final optimized wing shapes. Typically, for airfoil/wing single point shape optimization problems, a 'bump' is observed in the final optimized airfoil shape in the vicinity of the shock location for the baseline geometry [13]. For the OWN problem, if single point optimization were to be performed for the wing, one would expect differences in the decoupled and coupled optimized geometries in this region. That being said, single point optimized shapes are known to have significant off-design drag penalties. Multi-point design/optimization considers multiple flight conditions, and is recommended for obtaining smoother geometries that are robust to changes in flight condition and the associated change in shock location [13].

### C. Comparison of Coupling Variables

Results in the preceding subsections showed a minimal impact of the propulsion system on the aerodynamic characteristics of the airframe. In this subsection, changes in the propulsion coupling variables as a result of changes in the aerodynamic outputs is presented. Fig.11a shows the *absolute* percentage difference between

the engine boundary conditions from the coupled and decoupled analysis as a function of angle of attack. Dashed lines represent temperatures, while solid lines represent pressures. Fan face conditions are shown using diamond points, core nozzle inlet conditions are shown with squares, and bypass nozzle inlet conditions are shown with circles. The change in thrust required is also presented as a function of angle of attack to provide context to the boundary conditions. Fig. 11b shows the *absolute* percentage difference between the coupled and decoupled aerodynamic outputs as a function of angle of attack.

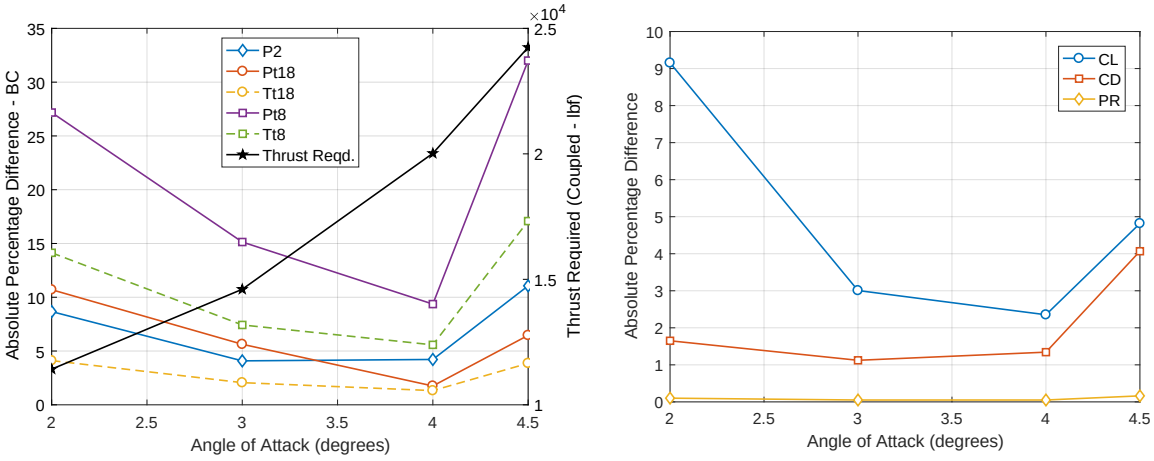


(a) Engine Boundary Conditions

(b) Aerodynamic Outputs

Figure 11: Absolute % difference between decoupled and coupled propulsion and aerodynamic outputs

From these figures, it is apparent that small changes in drag and pressure recovery result in much larger changes in the engine boundary conditions. Aerodynamic effects on the propulsion system are much stronger than the propulsion effects on aerodynamics, consistent with the findings in Ref. [8].

## IV. Conclusion

The goal of this paper was to extend previously conducted work that investigated aerodynamics-propulsion sensitivity for OWN configurations [8]. Statistically significant sensitivity was observed in that study, however, it was found that airframe aerodynamics had a stronger impact on the propulsion system than the reverse interaction. This paper aimed to quantify the differences in the aerodynamic coefficients as a result of capturing the coupling at a trailing edge configuration, for a varying angle of attack. The paper also hoped to answer whether conducting MDAO was necessary for this configuration. A comparison of $C_D$, $C_L$, and $\eta_{PR}$ coupled and decoupled trends as a function of flight condition (Fig. 6 and 11) showed that the propulsion system effects on the aerodynamics are weak, consistent with previous observations. Differences in the trends are larger at $\alpha = 2$ and $\alpha = 4.5$, however, at the CRM flight condition of $C_L = 0.5$, differences in $C_L$ and $C_D$ trends are less than 3%. Though differences in the aerodynamic coefficients are small, it was found that the shock location in the coupled case was further downstream than that for the decoupled case, at $\alpha = 4.5$. If the objective is to assess the drag reduction possible as a result of shape optimization, then MDAO is not necessary for this nacelle location. If obtaining the optimized wing shapes are of greater concern, and single point optimization is conducted, then MDAO is recommended since optimized airfoil shapes are sensitive to the shock location. That being said, if wing shape design is the primary focus, then a multi-point formulation is recommended for future work. Considering multiple flight conditions in the design problem is critical in obtaining an optimum geometry that is robust to changes in flight condition and thus shock location.

## References


[1] Fayette Collier. Environmentally responsible aviation project real solutions for environmental challenges facing aviation, 2012.

[2] R Owens, K Hasel, and D Mapes. Ultra high bypass turbofan technologies for the twenty-first century. In *26th Joint Propulsion Conference*, page 2397, 1990.

[3] Gerald L Brines. The turbofan of tomorrow. *Mechanical Engineering*, 112(8):65, 1990.

[4] John R. Hooker, Andrew Wick, Cale Zeune, and Anthony Agelastos. Over wing nacelle installations for improved energy efficiency. In *31st AIAA Applied Aerodynamics Conference*.

[5] Steven H Berguin. *A Method for Reducing Dimensionality In Large Design Problems With Computationally Expensive Analyses*. PhD thesis, Gerogia Institute of Technology, 2015.

[6] Lawrence E Putnam. Exploratory Investigation at Mach Numbers from 0.40 to 0.95 of the Effects of Jets Blown over a Wing. *Nasa Tn D-7367*, (November), 1973.

[7] David E Reubush. Effect of Over-the-Wing Nacelles on Wing-Body Aerodynamics. *Journal of Aircraft*, 16(6):359–365, 1979.

[8] Steven H. Berguin, Sudharshan Ashwin Renganathan, Jai Ahuja, Mengzhen Chen, Jimmy Tai, and Dimitri N. Mavris. Sensitivity analysis of aero-propulsive coupling for over-wing-nacelle concepts. In *AIAA SciTech Forum*. AIAA.

[9] Melissa B. Rivers and Ashley Dittberner. Experimental Investigations of the NASA Common Research Model. *Journal of Aircraft*, 51(4):1183–1193, 2014.

[10] John Vassberg, Mark Dehaan, Melissa Rivers, and Richard Wahls. Development of a Common Research Model for Applied CFD Validation Studies. *26th AIAA Applied Aerodynamics Conference*, (August):1–22, 2008.

[11] M. Kirby and D. Mavris. The environmental design space. In *26th International Congress of the Aeronautical Sciences*, Anchorage, Alaska, 14 - 19 September 2008.

[12] Michimasa Fujino, H. Oyama, and H. Omotani. chapter Flutter Characteristics of an Over-the-Wing Engine Mount Business-Jet Configuration. Structures, Structural Dynamics, and Materials and Colocated Conferences. American Institute of Aeronautics and Astronautics, Apr 2003.

[13] Mark Drela. *Pros and Cons of Airfoil Optimization*. World Scientific, 1998.